Structure and properties of $[(CH_3)_4P]_3[Sb_2Cl_9]$ and $[(CH_3)_4P]_3[Bi_2Cl_9]$

2004 J. Phys.: Condens. Matter 16 7521

(http://iopscience.iop.org/0953-8984/16/41/029)

INSTITUTE OF PHYSICS PUBLISHING JOURNAL OF PHYSICS: CONDENSED MATTER

J. Phys.: Condens. Matter **16** (2004) 7521–7534 PII: S0953-8984(04)81837-X

Structure and properties of $[(CH_3)_4P]_3[Sb_2Cl_9]$ and $[(CH_3)_4P]_3[Bi_2Cl_9]$

M Wojtaś[1] **and R Jakubas**

Faculty of Chemistry, University of Wrocław, Joliot-Curie 14, 50-383 Wrocław, Poland

E-mail: maciekwo@wcheto.chem.uni.wroc.pl

Received 8 June 2004, in final form 12 August 2004
Published 1 October 2004
Online at stacks.iop.org/JPhysCM/16/7521
doi:10.1088/0953-8984/16/41/029

Abstract

Two new phosphonium chloroantimonate(III) and chlorobismuthate(III) crystals ($[(CH_3)_4P]_3[Sb_2Cl_9]$ (PCA) and $[(CH_3)_4P]_3[Bi_2Cl_9]$ (PCB)) have been synthesized and their structure determined by means of single-crystal x-ray diffraction. The structure of the title compounds contains discrete $[M_2Cl_9]^{3-}$ anions in general positions and disordered $[(CH_3)_4P]^+$ cations. The two compounds are isomorphous in the room temperature phase and crystallize in the polar trigonal space group, $P31c$. The phase situation in PCA and PCB is established on the basis of differential scanning calorimetry and dilatometric studies. Two phase transitions are found: at 534/534 K (I $\leftrightarrow$ II) and at 135/138 K (II $\leftrightarrow$ III) for PCA and at 550/550 K (I $\leftrightarrow$ II) and at 151/155 K (II $\leftrightarrow$ III) for PCB (on cooling/heating). The values of the transition entropies (ΔS_{tr}) obtained suggest that the II $\rightarrow$ III transitions are of the order–disorder type. The dielectric dispersion measurements have revealed a relaxation process in the PCB crystal. The pyroelectric measurements of both compounds have confirmed the polar nature of the low temperature phase (III). The ferroic (ferroelastic) properties were found over phase III for both crystals.

1. Introduction

Investigations of compounds possessing organic cations and inorganic anions are of value not only because they provide interesting supramolecular networks; the supramolecular networks become especially interesting when the cation and the anion can participate in hydrogen bonding. The hydrogen bond configuration is usually recognized as the most powerful force for generating supramolecular assemblies of molecules. The halogenoantimonates(III) and halogenobismuthates(III) of general formula $R_aM_bX_{(3b+a)}$ (R = alkylammonium cations; M = Sb and Bi; X = Cl, Br, I) are examples of such systems exhibiting interesting ferroic

[1] Author to whom any correspondence should be addressed.

(ferroelastic, ferroelectric) properties and incommensurate modulated phases [1–6]. Among the salts, which are characterized by various anionic forms, the ones with the $R_3M_2X_9$ and $R_5M_2X_{11}$ compositions deserve special attention because they demonstrate ferroelectric and ferroelastic properties. Their anionic $[M_2X_9]^{3-}$ sublattice is built of: (i) one-dimensional zigzag chains [7], (ii) two-dimensional layers [8], (iii) discrete bioctahedra [9]. It was shown that ferroelectricity is limited to salts with small sized cations such as $(CH_3NH_3)^+$, $[(CH_3)_2NH_2]^+$ and $[(CH_3)_3NH]^+$ embedded in a layered anionic structure (type (ii)). The $R_5M_2X_{11}$-type salts are extremely rare [10] and only three examples of compounds (pyridinium and methylammonium) crystallizing with this composition are known so far. It is interesting that all $R_5M_2X_{11}$ salts exhibit ferroelectric properties. Both kinds of these crystals are classified as order–disorder ferroelectrics for which the mechanism of phase transitions is governed by the dynamics of organic cations. Quite recently, a novel ferroelectric with $RSbCl_4$ composition, i.e. 4-$NH_2PyHSbCl_4$, characterized by a one-dimensional anionic form, $(SbCl_4)^-_\infty$, has been discovered [11].

In the case of salts with $R_3M_2X_9$ composition it was shown that the type of structure adopted by $[M_2X_9]^{3-}$ anions depends on the size of the cations and the possibility of specific interactions with the anion. Large bulky cations such as tetramethylammonium inhibit the formation of a polymeric anion in the crystal lattice and, as a result, only discrete bioctahedral anionic structure is formed. Many phase transitions in tetramethylammonium salts belonging to the $R_aM_bX_{(3b+a)}$ family studied so far lead, as a rule, to the low temperature ferroelastic phases. The tetramethylammonium salts of our system are characterized by rather weak dipole–dipole interactions, so the possibility of ferroelectricity is undoubtedly excluded.

In the search for new polar crystals we have synthesized two tetramethylphosphonium analogues, $[(CH_3)_4P]_3[Sb_2Cl_9]$ and $[(CH_3)_4P]_3[Bi_2Cl_9]$. In this paper we report on crystal structure, differential scanning calorimetry (DSC), dilatometry, dielectric and pyroelectric studies of these crystals. The mechanism of the ferroelastic–paraelastic phase transitions in tetramethylphosphonium analogues is discussed.

2. Experimental details

The powder of tris(tetramethylphosphonium) nonachlorodiantimonate (III) ($[(CH_3)_4P]_3[Sb_2Cl_9]$ (PCA)) and tris(tetramethylphosphonium) nonachlorodibismuthate (III) ($[(CH_3)_4P]_3[Bi_2Cl_9]$ (PCB)) was obtained by reaction of $[(CH_3)_4P]Cl$ and $SbCl_3$ or $BiCl_3$ in a concentrated hydrochloric acid. The single crystals of PCA or PCB were grown by slow evaporation of an aqueous solution at room temperature. The crystals grow with a pseudo-hexagonal habit and have a well-developed (001) plane.

Crystal data are given in table 1, together with refinement details. All measurements on the crystals were performed on a Kuma KM4CCD κ-axis diffractometer with graphite-monochromated Mo Kα radiation. The crystals were positioned at 65 mm from a KM4CCD camera. 612 frames were measured at 0.75° intervals with a counting time of 20 s. The data were corrected for Lorentz and polarization effects. Analytical absorption corrections and the data reduction and analysis were carried out with the Oxford Diffraction (Poland) programs. The structures were solved by the heavy atom method (program SHELXS97 [12]) and refined by the full-matrix least squares method applied to all F^2 data using the SHELXL97 [13] programs. Non-hydrogen atoms were refined with anisotropic displacement parameters; hydrogen atoms were included from the geometry of the molecules and $\Delta\rho$ maps were fixed.

Crystallographic data for the structures reported in this paper (excluding structure factors) have been deposited in the Cambridge Crystallographic Data Centre, CCDC Nos 232592 (PCA) and 232593 (PCB). Copies of this information may be obtained free of charge from the

Table 1. Crystal data and the structure refinement for $[(CH_3)_4P]_3[Sb_2Cl_9]$ and $[(CH_3)_4P]_3[Bi_2Cl_9]$.

Empirical formula	$[(CH_3)_4P]_3[Sb_2Cl_9]$	$[(CH_3)_4P]_3[Bi_2Cl_9]$
Formula weight	835.87	1010.33
Temperature (K)	293(2)	180(2)
Wavelength (Å)	0.710 73	
Crystal system	Trigonal	
Space group	$P31c$	
Unit cell dimensions (Å)	$a = 9.4270(6)$	$a = 9.4490(6)$
	$c = 22.174(2)$	$c = 22.194(2)$
Volume (Å^3)	1706.6(2)	1716.1(2)
Z	2	
Calculated density (g cm^{-3})	1.627	1.955
Absorption coefficient (mm^{-1})	2.430	11.082
$F(000)$	816	944
Crystal size (mm)	$0.10 \times 0.10 \times 0.10$	$0.10 \times 0.10 \times 0.10$
Theta range for data collection (deg)	3.68–28.57	3.09–28.52
Ranges of h, k, l	$-10 \Rightarrow 12, -12 \Rightarrow 10, -28 \Rightarrow 28$	$-12 \Rightarrow 12, -10 \Rightarrow 12, -28 \Rightarrow 23$
Reflections collected	11 403	11 265
Independent reflections (R_{int})	2751 (0.0656)	2503 (0.0864)
Absorption correction	Analytical	
Data/parameters	2751/79	2503/79
Goodness-of-fit on F^2	1.141	1.064
Final R_1/wR_2 indices ($I > 2\sigma I$)	0.0694/0.0843	0.0508/0.0785
Largest diff. peak/hole (e Å^{-3})	0.423/−0.505	0.860/−0.701

Director, CCDC, 12 Union Road, Cambridge, CB2 1EZ, UK (fax: +44-1223-336033; e-mail: deposit@ccdc.cam.ac.uk, http://www.ccdc.cam.ac.uk).

The complex electric permittivity, $\epsilon^* = \epsilon' - i\epsilon''$, was measured with HP 4284 and HP 4285A Precision LCR Meters within the frequency range 1 kHz–25 MHz and in the temperature range 100–400 K. The dimensions of the sample were of the order of $3 \times 3 \times 1$ mm^3. The overall error for the real and imaginary parts of the complex electric permittivity was less than 5% and 10%, respectively.

The spontaneous polarization was measured by a charge integration technique using a Keithley 617 programmable electrometer. The temperature was stabilized by an Instec STC200 temperature controller.

Differential scanning calorimetry (DSC) measurements were carried out using a Perkin-Elmer DSC-7 in the temperature range 100–600 K.

The dilatometric measurements were made using a thermomechanical analyser, Perkin-Elmer TMA-7, within the temperature range 100–600 K at a scanning rate of 2 K min^{-1}. The dimensions of the sample were of the order of $2 \times 3 \times 1$ mm^3.

The ferroelastic domain structure of the crystal was studied by means of an OLYMPUS (BX60 SYSTEM) optical polarization microscope. The samples were placed on a LINKAM THM-600 heating–cooling stage where the temperature was stabilized to within 0.01 K.

3. Results and discussion

3.1. X-ray results

The final atomic coordinates of PCA and PCB are listed in table 2. The asymmetric part of the unit cell consists of one discrete bioctahedral $[M_2Cl_9]^{3-}$ unit and three symmetrically

Table 2. Atomic coordinates and equivalent isotropic displacement parameters (Å^2) for $[(CH_3)_4P]_3[Sb_2Cl_9]$ and $[(CH_3)_4P]_3[Bi_2Cl_9]$. U_{eq} is defined as one third of the trace of the orthogonalized U_{ij} tensor.

Atom	x	y	z	U_{eq}
		$[(CH_3)_4P]_3[Sb_2Cl_9]$		
Sb(1)	0.6667	0.3333	0.380 17(3)	0.0558(4)
Sb(2)	0.6667	0.3333	0.551 77(3)	0.0531(4)
Cl(1)	0.5869(3)	0.5166(3)	0.465 5(2)	0.1128(10)
Cl(2)	0.7335(4)	0.1601(4)	0.317 29(15)	0.0966(9)
Cl(3)	0.4271(3)	0.2655(4)	0.614 80(15)	0.0969(9)
P(1)	0.3333	0.6667	0.628 0(3)	0.0609(19)
P(2)	0.3333	−0.3333	0.306 1(3)	0.0493(16)
P(3)	1.0000	1.0000	0.465 6(4)	0.0690(9)
C(11)	0.3333	0.6667	0.547 7(14)	0.109(9)
C(12)	0.1853(13)	0.4715(12)	0.653 1(6)	0.101(4)
C(21)	0.3333	−0.3333	0.384 2(8)	0.109(9)
C(22)	0.2883(15)	−0.1865(14)	0.277 2(6)	0.104(4)
C(31)	1.0486(11)	0.8509(11)	0.469 3(13)	0.195(7)
C(32)	1.0000	1.0000	0.547 8(12)	0.29(2)
		$[(CH_3)_4P]_3[Bi_2Cl_9]$		
Bi(1)	0.3333	0.6667	0.622 58(3)	0.0350(4)
Bi(2)	0.3333	0.6667	0.448 86(3)	0.0340(4)
Cl(1)	0.4115(3)	0.4867(3)	0.536 17(15)	0.0405(7)
Cl(2)	0.2637(5)	0.8495(5)	0.686 71(17)	0.0617(10)
Cl(3)	0.5879(5)	0.7359(5)	0.385 69(17)	0.0606(10)
P(1)	0.6667	0.3333	0.373 6(4)	0.035(2)
P(2)	0.6667	1.3333	0.698 7(4)	0.032(2)
P(3)	0.0000	0.0000	0.539 0(6)	0.0442(14)
C(11)	0.6667	0.3333	0.445 4(15)	0.043(8)
C(12)	0.8206(17)	0.5277(16)	0.347 1(7)	0.062(4)
C(21)	0.6667	1.3333	0.610 6(15)	0.041(8)
C(22)	0.7084(17)	1.1780(17)	0.725 8(6)	0.054(4)
C(31)	0.0000	0.0000	0.625 6(8)	0.28(4)
C(32)	0.202(2)	0.070(3)	0.515 9(11)	0.234(19)

inequivalent tetramethylphosphonium cations (see figure 1). The anionic structure within the *ac*-plane is shown as a polyhedral representation in figure 2. The enlargement of the thermal parameters of the carbon atoms indicates significant disorder within the cationic sublattice. The disorder was not resolvable and was also responsible for the impossibility of refining for the tetramethylphosphonium cation with the P(3) atom. The P(3)–C bonds and C–P(3)–C angles were fixed and they are not included in table 3.

Because of the high symmetry, the $[M_2Cl_9]^{3-}$ anions are defined by only two metal–chlorine distances associated with the bridging and terminal atoms, respectively. The bond lengths and the angle values are typical for similar structures reported in the literature [9, 14]. The Sb–$Cl_{terminal}$ and Sb–$Cl_{bridging}$ bond lengths are equal to 2.457(3)/2.453(3) Å (for Sb(1)/Sb(2)) and 2.904(4)/2.917(3) Å, respectively. The equivalent Bi–Cl bonds are longer by 0.108(3)/0.117(3) Å for terminal bonds, but slightly shorter, by 0.010(3)/0.010(3) Å, for bridging ones (for Bi(1)–Sb(1)/Bi(2)–Sb(2) atoms). It should be kept in mind here that the structure of PCB was measured at 180 K, whereas the structure of PCA was determined at room temperature (293 K).

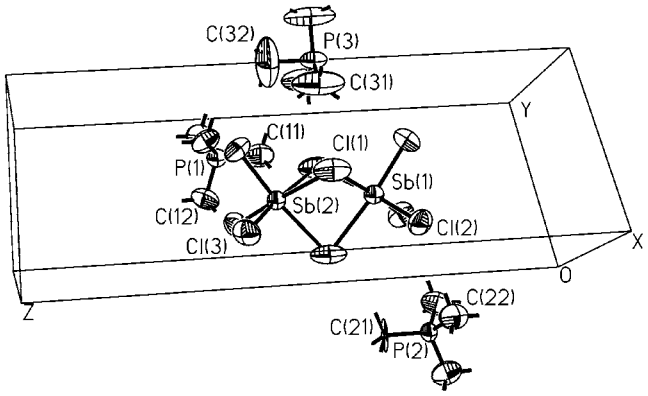

Figure 1. A perspective view of the asymmetric part of the unit cell of $[(CH_3)_4P]_3[Sb_2Cl_9]$ along the *a*-axis.

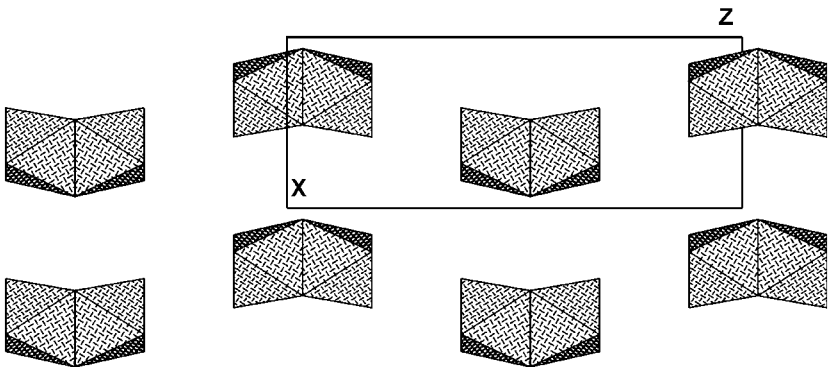

Figure 2. Discrete $[M_2Cl_9]^{3-}$ units in a polyhedral representation within the *ac*-plane.

3.2. Thermal behaviour of PCA and PCB

The DSC curves obtained for the PCA and PCB crystals in the low and high temperature regions during either heating or cooling scans are presented in figures 3(a) and (b), respectively. Hereafter, the following phases are denoted as phase I, phase II and phase III from the high temperature side. The high temperature phase transition I $\rightarrow$ II is continuous in nature, whereas the low temperature one, II $\rightarrow$ III, is clearly discontinuous. Both transitions are readily reversible and the II $\rightarrow$ III transition is characterized by rather small temperature hysteresis. The temperature of the phase transitions and the associated entropy changes as well as the temperature hystereses are presented in table 4.

The thermal hysteresis was estimated from scans performed at various rates (3–20 K min^{-1}) extrapolated to a scanning rate of 0 K min^{-1}. The continuous character of the I $\rightarrow$ II phase transition is also confirmed by the shape of the heat anomaly (characteristically λ shaped) and the lack of a steplike anomaly in the dilation for both crystals. (By 'λ shaped', we mean that the DSC scans show a definite low temperature tail.)

Figure 4 shows the results for the linear thermal expansion, $\Delta L/L_0$, measured along the main crystallographic axes of the trigonal system, *a* and *c*. These data sets agree well with results obtained by the DSC technique: the high temperature phase transition is manifested only as a very subtle inflection of the baseline, and the low temperature phase transition is

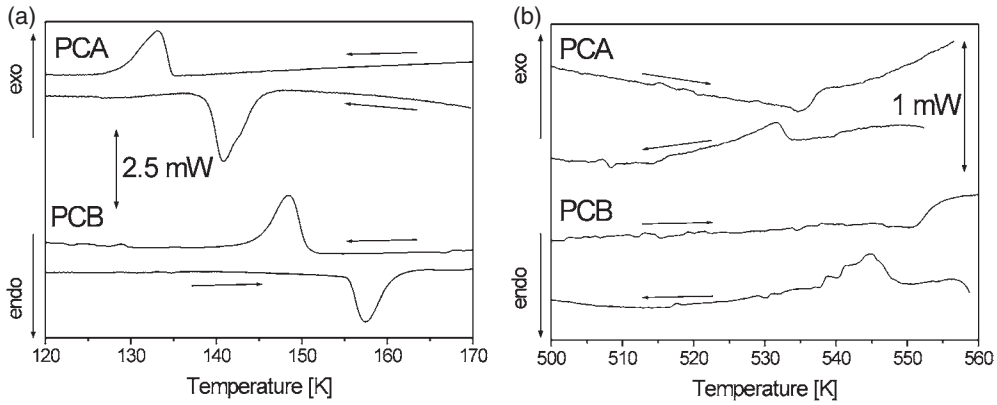

Figure 3. DSC curves of the PCA and PCB crystals for the (a) low and (b) high temperature regions, for the cooling and heating runs (10 K min^{-1}).

Table 3. Selected bond lengths (Å) and angles (deg) for $[(CH_3)_4P]_3[Sb_2Cl_9]$ and $[(CH_3)_4P]_3[Bi_2Cl_9]$.

$[(CH_3)_4P]_3[Sb_2Cl_9]$			
Sb(1)–Sb(2)	3.805(1)	Sb(1)–Cl(1)–Sb(2)	81.64(6)
Sb(1)–Cl(2)	2.457(3)	Cl(1)–Sb(1)–Cl(2) No 4	94.16
Sb(1)–Cl(1)	2.904(4)	Cl(1)–Sb(1)–Cl(2)	173.78(11)
Sb(2)–Cl(1)	2.917(3)	Cl(1)–Sb(2)–Cl(3)	92.95(11)
Sb(2)–Cl(3)	2.453(3)	Cl(1)–Sb(2)–Cl(3) No 4	173.69(11)
P(1)–C(11)	1.78(3)	C(12)–P(1)–C(11)	108.5(5)
P(1)–C(12)	1.754(10)	C(12)–P(1)–C(12) No 4	110.4(4)
P(2)–C(21)	1.73(2)	C(21)–P(2)–C(22)	111.3(5)
P(2)–C(22)	1.759(10)	C(22)–P(2)–C(22) No 6	107.5(5)
$[(CH_3)_4P]_3[Bi_2Br_9]$			
Bi(1)–Bi(2)	3.855(1)	Bi(1)–Cl(1)–Bi(2)	83.32(7)
Bi(1)–Cl(2)	2.565(3)	Cl(2)–Bi(1)–Cl(1) No 1	92.32(12)
Bi(1)–Cl(1)	2.894(3)	Cl(2)–Bi(1)–Cl(1)	172.08(11)
Bi(2)–Cl(3)	2.570(3)	Cl(3)–Bi(2)–Cl(1)	91.91(11)
Bi(2)–Cl(1)	2.907(3)	Cl(3)–Bi(2)–Cl(1) No 2	171.13(11)
P(1)–C(11)	1.60(3)	C(11)–P(1)–C(12)	109.3(6)
P(1)–C(12)	1.778(13)	C(12)–P(1)–C(12) No 4	109.6(6)
P(2)–C(21)	1.95(3)	C(22)–P(2)–C(21)	109.4(5)
P(2)–C(22)	1.803(13)	C(22)–P(2)–C(22) No 6	109.5(5)

Symmetry transformations used to generate equivalent atoms:
No 1: $-y+1, x-y+1, z$; No 2: $-x+y, -x+1, z$;
No 3: $-x+y+1, -x+1, z$; No 4: $-y+1, x-y, z$;
No 5: $-y+2, x-y+2, z$; No 6: $-x+y, -x+2, z$;
No 7: $-x+y, -x, z$; No 8: $-y, x-y, z$

characterized by a stepwise change of the crystal dimensions. It should be noted that the observed anomalies related to the II → III phase transition along the *a* and *c* directions are positive. The pressure coefficient for this first-order phase transition is estimated from the Clausius–Clapeyron equation:

$$\frac{dT_c}{dp} = \frac{\Delta V}{\Delta S}, \tag{1}$$

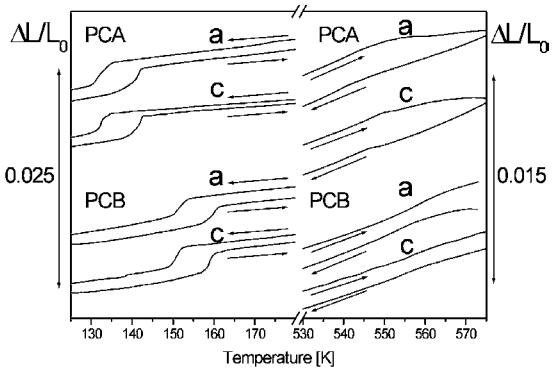

Figure 4. The linear thermal expansion of the PCA and PCB crystals.

Table 4. Structural phase transitions in the $[(CH_3)_4P]_3[Sb_2Cl_9]$ (PCA) and $[(CH_3)_4P]_3[Bi_2Cl_9]$ (PCB) crystals detected by DSC and dilatometric measurements. (Note: T_c, ΔT and ΔS stand for the transition temperature (during cooling), temperature hysteresis and entropy of the phase transition, respectively. In the lower part of the table we give the changes of the linear thermal expansion along the a and c directions and the pressure coefficients dT_c/dp.)

Compound	PCA			PCB		
phase transition	T_c (K)	ΔT (K)	ΔS (J mol^{-1} K^{-1})	T_c (K)	ΔT (K)	ΔS (J mol^{-1} K^{-1})
I → II	534	—	—	550	—	—
II → III	135	3.5	13.7	151	4.0	8.8
			Dilatometry			
	Axis	$\Delta L/L_0$	dT_c/dp (K MPa^{-1})	Axis	$\Delta L/L_0$	dT_c/dp (K MPa^{-1})
II → III	a	1.8×10^{-3}	19×10^{-2}	a	1.4×10^{-3}	25×10^{-2}
	c	1.5×10^{-3}		c	1.5×10^{-3}	

where ΔV denotes the change in the molar volume and ΔS is the value of the transition entropy. The magnitudes of the anomalies in the dilation along the a- and c-axes and the pressure coefficients for PBA and PBB are collected in table 4.

3.3. Dielectric properties

The purpose of the dielectric dispersion measurements was to determine the dynamics of the dipole groups (distorted tetramethylphosphonium cations) around the structural phase transitions at low temperature for both title compounds. The measurements of the complex electric permittivity, ϵ^*, for $[(CH_3)_4P]_3[Bi_2Cl_9]$ (PCB) and $[(CH_3)_4P]_3[Sb_2Cl_9]$ (PCA), as a function of temperature and frequency (75 kHz–25 MHz) were performed along the a- and c-axes during cooling. Figure 5 shows the temperature dependence of the real parts of the complex electric permittivity, ϵ'_a and ϵ'_c, for the PCA crystal in the vicinity of the phase transition at 135 K (on cooling). At the phase transition temperature we observe discontinuous change in both the ϵ'_a and ϵ'_c values. The observed dielectric increments, $\Delta\epsilon'_a = 1$ and $\Delta\epsilon'_c = 0.5$, are relatively small. The dielectric increment, $\Delta\epsilon'_c$, is independent of the applied frequency of the electric field, whereas $\Delta\epsilon'_a$ is weakly frequency dependent. Such a dielectric response, $\Delta\epsilon(T)$, is typical of a first-order phase transition, which is in agreement with the DSC and dilatometric results. A quite similar dielectric response is found for the PCB crystal.

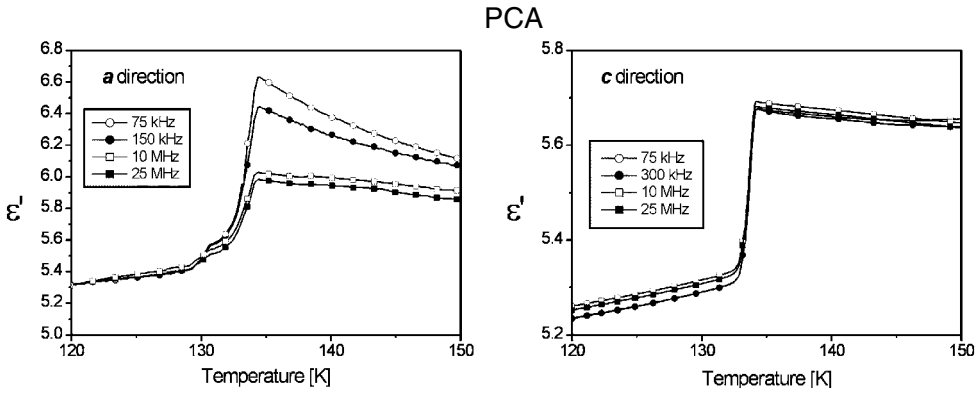

Figure 5. The temperature dependence of the real parts of the complex electric permittivity, ϵ'_a and ϵ'_c, for the PCA crystal in the vicinity of the phase transition at 135 K (on cooling).

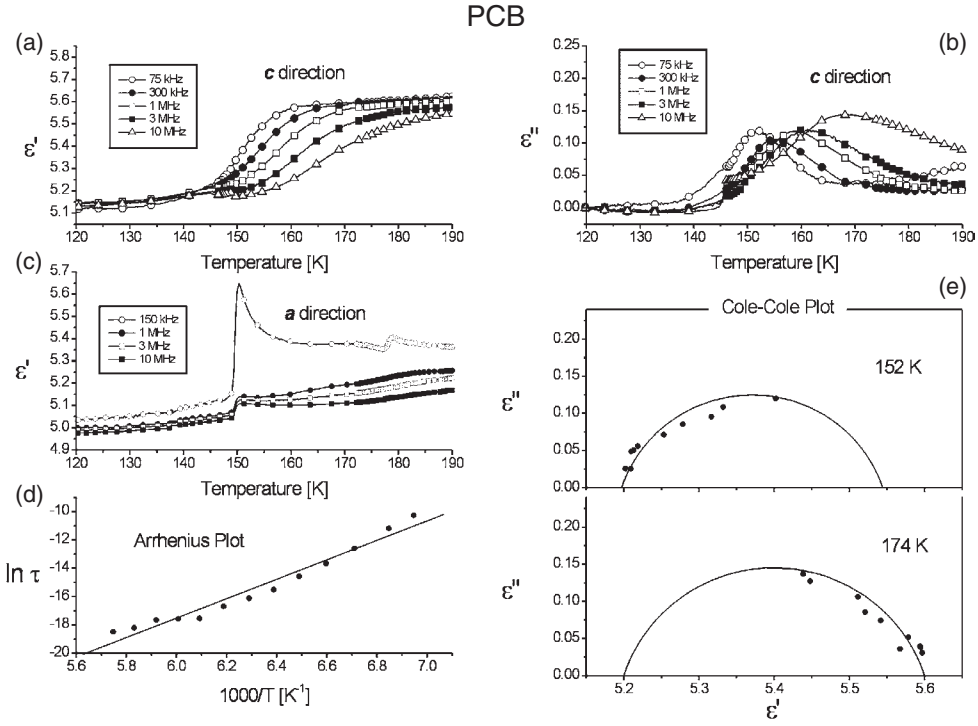

Figure 6. The temperature dependence of: (a) the real and (b) the imaginary part of the complex electric permittivity, ϵ^*_a, (c) the real part of the complex electric permittivity, ϵ'_c, and (d) $\ln \tau$ for the PCB crystal in the vicinity of the phase transition at 151 K; (e) the hypothetical Cole–Cole plots for two temperatures: 152 and 174 K.

Figures 6(a)–(c) show ϵ'_a, ϵ'_c and ϵ''_c versus temperature in the frequency range between 75 kHz and 10 MHz. The dielectric relaxation process is more clearly visible along the c direction. The dielectric response in the PCB salt is well described by the classical Debye relation:

$$\epsilon^* = \epsilon_\infty + \frac{\epsilon_0 - \epsilon_\infty}{1 + \mathrm{i}\omega\tau}, \tag{2}$$

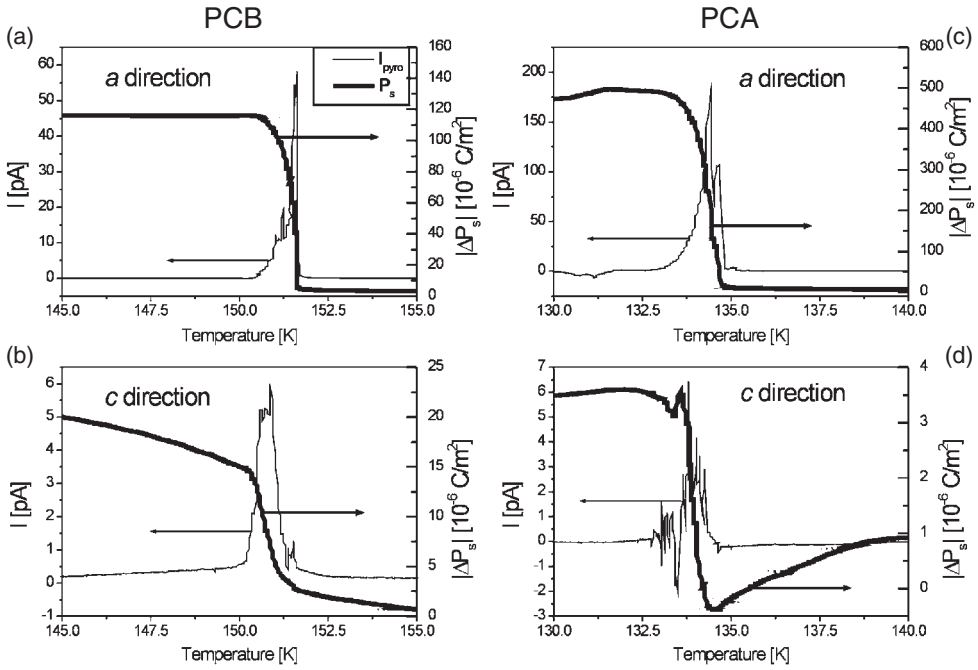

Figure 7. The temperature dependence of the pyroelectric current, I_{pyro}, and the spontaneous polarization change, ΔP_s, measured along the a- and c-axes of the $[(CH_3)_4P]_3[Sb_2Cl_9]$ ((a), (b)) and $[(CH_3)_4P]_3[Bi_2Cl_9]$ ((c), (d)) crystals, respectively.

where ϵ_0 and ϵ_∞ are the low and high frequency limits of the electric permittivity, respectively, ω is the angular frequency, τ is the macroscopic relaxation time.

The Argand diagrams at selected temperatures, above the phase transition temperature $T_c = 151$ K, are presented in figure 6(e). We have fitted the experimental Argand plots at several temperatures with equation (2) and determined the fitting parameters ϵ_0, ϵ_∞ and τ. The activation energy, E_a, was estimated from the Arrhenius relation for the relaxation time:

$$\tau = C \exp\left(\frac{E_a}{kT}\right), \tag{3}$$

where C is a constant. This activation energy estimated for the relaxation process (see figure 6(d)) is equal to 9 kJ mol^{-1} and is typical for ionic crystals containing organic cations of large size.

3.4. Pyroelectric properties

To throw more light on the polar properties of PCA and PCB in the vicinity of the paraelastic–ferroelastic phase transition, pyroelectric measurements have been carried out. The x-ray studies showed that the intermediate phase II (paraelastic) possesses polar character (noncentrosymmetric space group, $P31c$). Since the pyroelectric method does not allow us to determine the absolute value of P_s for the phases II and III, only the changes in the spontaneous polarization $|\Delta P_s|$ at $T_c(\text{II} \rightarrow \text{III})$ have been detected. The spontaneous polarizations as a function of temperature along the a- and c-axes of PCB are shown in figures 7(a), (b). It is seen that the $|\Delta P_s|$ change along the a-axis in the vicinity of 151 K, being of the order of 1.2×10^{-4} C m^{-2}, is nearly one order higher than that along the c-axis. The pyroelectric properties of PCA in the vicinity of the II $\rightarrow$ III PT are illustrated in figures 7(c), (d). Similarly

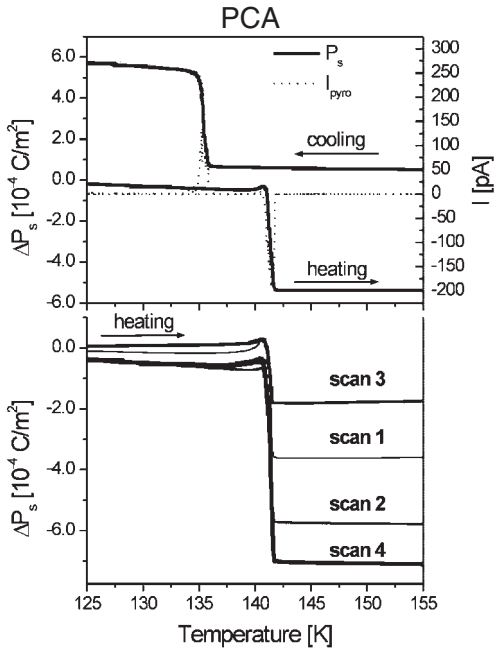

Figure 8. Upper: the temperature dependence of the spontaneous polarization change, ΔP_s, and the pyroelectric current measured along the a-axis of the $[(CH_3)_4P]_3[Sb_2Cl_9]$ crystal, for cooling and heating. Lower: the temperature dependence of the spontaneous polarization, ΔP_s, for the poling fields +500 V (scan 1), −500 V (scan 2), +1000 V (scan 3) and −1000 V (scan 4).

to in the case of PCB, for the antimony analogue (PCA) in the vicinity of the 135 K PT the largest pyroelectric current was recorded along the a-axis. Figure 8 shows the dependences of the ΔP_s changes and the pyroelectric current along the a-axis on temperature for the cooling and heating scans of the sample, which was not poled before the measurements. The pyroelectric current is perfectly reversed during the cooling and heating scans, which confirms the pyroelectric character of the transition II → III.

To check whether the spontaneous polarization is reversed under an external DC electric field, the sample was poled with fields of −500, −1000, +500 and +1000 V. The sample was cooled, for each experiment under an applied DC electric field, starting from 155 K down to 125 K. The pyroelectric measurements were performed on heating. The results are summarized in figure 8. The DC field of +500 V yields a ΔP_s at T_c(II → III) of about 3.5×10^{-4} C m^{-2}, which is smaller than that for the sample without any poling. Next, an electric field of −500 V was applied, giving an increase in the ΔP_s value to 5.5×10^{-4} C m^{-2}. The higher but positive electric field, +1000 V, again decreases ΔP_s, to 1.5×10^{-4} C m^{-2}, whereas the strongest negative DC field −1000 V yields the largest ΔP_s at T_c, of the order of 7×10^{-4} C m^{-2}. We can conclude that the external DC electric field strongly influences the polar properties of the crystal in the vicinity of the II → III PT. Such behaviour may be explained in terms of the presence of domain structure below 135 K. It should also be added that the P_s value close to 1×10^{-3} C m^{-2} is rather typical for 'weak' ferroelectric crystals, whereas most of the nonferroelectric pyroelectric materials exhibit P_s values of the order of 1×10^{-5}–10^{-6} C m^{-2}. The DC field (10 kV cm^{-1}) applied by us appeared to be too low to reverse the spontaneous polarization in phase III. The polar properties of the crystal were also checked with a Sawyer–Tower circuit. Unfortunately, we failed to observe any hysteresis loops up to 10 kV cm^{-1}

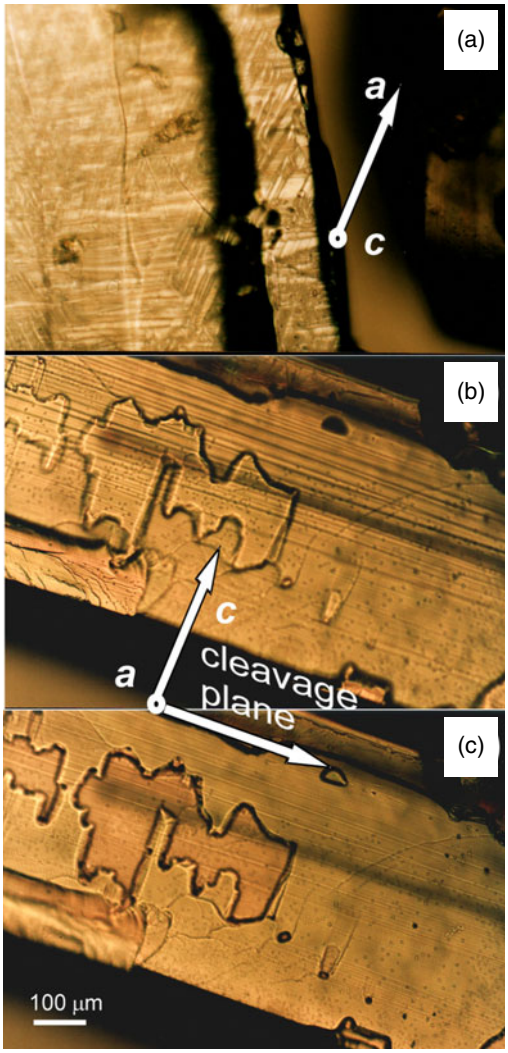

Figure 9. A micrograph of the ferroelastic domain structure between crossed polarizers taken along the *c*-axis of the PCA crystal at 120 K—phase III (a) and along the *a*-axis in the vicinity of T_c(III → II) at two selected temperatures: at 130 K—phase III (b) and at 155 K—phase II (c). (This figure is in colour only in the electronic version)

because of the too high coercive field. Nevertheless, the pyroelectric measurements allow us to state that $[(CH_3)_4P]_3[Sb_2Cl_9]$ (PCA) is potentially a ferroelectric material below 135 K.

3.5. Optical observations

PCA was observed under the polarizing microscope along the *c*-axis (see figure 9(a)) and the *a*-axis (figures 9(b), (c)) in the vicinity of the low temperature II → III phase transition (the directions correspond to those taken for the trigonal room temperature phase). Below the transition temperature ($T_c = 135$ K), in PCA one can observe platelike ferroelastic domains with walls parallel to the *a*-axis (figure 9(a)). The domain boundaries cross at an angle of 60° or 120°. The domain structure along the *a*-axis of the sample is displayed in figure 9(b). The

observed domains are positioned within the cleavage plane, which is perpendicular to the c-axis. Figure 9(c) shows the same sample of PCA crystal just above the T_c(III $\rightarrow$ II) temperature, confirming the disappearance of the domain structure. This process is perfectly reversible. This means that this transition may be classified as a ferroelastic one and should be accompanied by a change in the crystal symmetry. In the case of PCB the domain structure below 151 K is barely visible. On the basis of the optical observations and Sapriel's approach [15], one can state that the PCA and PCB crystals belong to the ferroelastic species with $3mFm$ or $3mF1$ domain patterns.

3.6. Group theoretical analysis of the phase transitions in PCA and PCB

The I $\rightarrow$ II phase transition in PCA and PCB is undoubtedly a nonferroelastic transition. This means that such a transition must take place between hexagonal or trigonal symmetry (I) and trigonal symmetry (II).

As the phase transition I $\rightarrow$ II is continuous, one should expect a group–subgroup relation between the space groups of the two phases: $G(\mathrm{I}) \supset G(\mathrm{II})$. Moreover, there should be no intermediate space group G' such that $G(\mathrm{I}) \supset G' \supset G(\mathrm{II})$. The above conditions are fulfilled by the following space groups: $P\overline{3}1c$ (D^2_{3d}), $P\overline{3}c1$ (D^4_{3d}), $P\overline{6}2c$ (D^4_{3h}) and $P\overline{6}c2$ (D^2_{3h}). The groups $P\overline{3}1c$ (D^2_{3d}), $P\overline{3}c1$ (D^4_{3d}) result from the addition of an inversion to the group $P31c$; the orientation of the twofold axes, which distinguishes the two groups, cannot be determined from knowledge of just the subgroup $P31c$. The groups $P\overline{6}2c$ (D^4_{3h}) and $P\overline{6}c2$ (D^2_{3h}) are a result of the addition of a mirror plane perpendicular to the threefold axis of the group $P31c$. The space group of the tetramethylammonium compounds $P6_3/mmc$ is the result of a simultaneous addition of both those elements and cannot be the space group of the parent phase if the phase transition is indeed continuous. All the groups mentioned above assume the same number of atoms in phases I and II (*zellengleich*). Under the same hypothesis, the most plausible space group of phase III is Cc (C^4_s). An increase in the number of atoms per unit cell is not probable in the phase transition II $\rightarrow$ III, because the micrographs show patterns indicating a proper rather than a pseudoproper ferroelastic behaviour.

3.7. Discussion

The tetramethylphosphonium analogues $[(CH_3)_4P]_3[M_2X_9]$ (M = Sb, Bi, X = Cl, Br) and closely related tetramethylammonium salts $[(CH_3)_4N]_3[M_2X_9]$ revealed a substantial similarity as regards structural and physical properties. Both subgroups crystallize in space groups characterized by high symmetry: tetramethylammonium—$P6_3/mmc$ and tetramethylphosphonium—$P31c$. Such high symmetry is connected with a significant dynamic disorder of the quaternary organic cations at room temperature. The common feature of the compared analogues is the presence of discrete bioctahedral anionic units $[M_2X_9]^{3-}$ in the crystal structure. The freezing of the reorientational motion of the cations leads to low temperature ordered phases. It should be emphasized that the low temperature transitions are connected with the generation of ferroic (ferroelastic) properties. The most important difference in phase situation between these two groups is the fact that at high temperatures (above 540 K) continuous phase transitions appear only in the tetramethylphosphonium salts. Starting from the highest temperature phase of the $[(CH_3)_4P]_3[M_2X_9]$ crystals, the I $\rightarrow$ II phase transition leads to a polar phase (space group $P31c$). This indicates that the dynamics of the organic cations responsible for the polar properties are different for these two classes of compounds.

Let us try to compare the phase situations within the tetramethylphosphonium analogues which are illustrated in table 5. The temperature of the I $\rightarrow$ II transitions ranges between 534

Table 5. Selected structural parameters, phase transitions, entropy transitions and spontaneous polarization changes in the tetramethylphosphonium analogues, $[P(CH_3)_4]_3[M_2X_9]$.

Crystal	$[(CH_3)_4P]_3[Sb_2Cl_9]$	$[(CH_3)_4P]_3[Bi_2Cl_9]$	$[(CH_3)_4P]_3[Sb_2Br_9]$	$[(CH_3)_4P]_3[Bi_2Br_9]$
V (Å^3)	1706.6 (293 K)	1716.1 (180 K)	1885.2 (293 K)	1895.0 (293 K)
a (Å)	9.4270(6)	9.4490(6)	9.7931(7)	9.7880(12)
c (Å)	22.174(2)	22.194(2)	22.6974(19)	22.840(4)
I → II PT continuous	534 K	550 K	540 K	550 K
II → III PT ferroelastic, discontinuous	135 K	151 K	193 K	205 K
ΔS(II → III) (J mol^{-1} K^{-1})	13.7	8.8	8.5	10.6
$\lvert P_s\rvert$ (10^{-5} C m^{-2}) at T_c(II → III)	50	12	2.5	0.5
direction	a-axis	a-axis	a-axis	c-axis

and 550 K. It is clearly seen that the metal substitution, Sb → Bi, weakly influences the phase transition temperature, by over a dozen degrees, whereas the halogen exchange, Cl → Br, practically does not shift the I → II transition temperature. The mechanism of this transition is still unclear, since we have only dilatometric and calorimetric results so far. Nevertheless, a 'displacive' mechanism for the I → II transitions seems possible in view of the relatively small entropy effect.

An interesting regularity for the phase transition sequence was observed for the paraelastic–ferroelastic transitions at low temperatures. The metal (Sb → Bi) replacement weakly affects the ferroelastic transition both for the chlorine (ΔT_c(II → III) = 16 K) and for the bromine (ΔT_c(II → III) = 12 K) analogue. A significant change in the T_c value is observed for the halogen (Cl → Br) exchange. The temperature of T_c(II → III) shifts upwards by about 58 and 54 K for the antimony and bismuth analogues, respectively. This unequivocally shows that the halogen atoms play a more important role in the dynamics of the organic cations, which are directly involved in the ferroelastic phase transition mechanism. It seems obvious that an increase in the van der Waals radius of the halogen atoms, when the Cl atom is replaced by the Br one, is reflected in the steric effect in the crystal lattice. So, for the bromine salts the reorientational motions of the cations should be frozen at higher temperatures in comparison to those in the corresponding chlorine ones, which is what is actually observed in our studies. It should be added that a similar tendency in the direction of the temperature shift of the ferroelastic transition is encountered in the $[(CH_3)_4N]_3[M_2X_9]$ subgroup.

The molecular mechanism of the low temperature transition seems to be common to the all tetramethylphosphonium $[(CH_3)_4P]_3[M_2X_9]$ salts. The dynamics of the organic cations has been studied in the case of $[(CH_3)_4P]_3[Sb_2Br_9]$ [16] using a ^{1}H NMR method. It was shown that in the lowest temperature phase III (below T_c(II → III)) the organic cations are 'frozen' as a whole, showing only the C_3-type motion of the methyl groups. Over the intermediate phase II the isotropic rotation of this cation was admitted. A similar mechanism for the paraelastic–ferroelastic phase transition is postulated on the basis of the present x-ray and dielectric studies in the title crystals. The isotropic disorder of the cations is reflected in the value of the isotropic displacement coefficients (U_{eq}) of the carbon atoms, especially for the cation type (3), which are of the order of 0.23–0.28 Å^2. This suggests a significant disorder of at least one of the

cations over several sites. Such a model of disorder is also confirmed by quite large entropy transitions accompanying the II $\rightarrow$ III phase transition (13.7 (Sb) and 8.8 (Bi) J mol^{-1} K^{-1}).

The common feature of the dielectric responses of the tetramethylphosphonium compounds is a relatively small jump in the electric permittivity value accompanying the paraelastic–ferroelastic phase transition. This may be explained by the fact that the organic tetramethylphosphonium cations have a small permanent electric dipole moment bestowed on them. So, the 'freezing' of the cation motions should lead to a change in the resultant dipole moment of the unit cell, which is reflected in the value of the dielectric increment ($\Delta\epsilon$). Moreover, it should be noted that both PCB and PBA reveal a dielectric relaxation process over phase II with a macroscopic relaxation time (τ) of about 10^{-4}–10^{-6} s. This process is assigned to the dynamics of polar organic cations. It confirms clearly the possibility of overall motions of the cations for temperatures above T_c(III $\rightarrow$ II), as was postulated from the ^{1}H NMR [16]. It should also be underlined that in the case of chlorine analogues the dielectric permittivity, especially along the a-axis, increases on approaching T_c(II $\rightarrow$ III), which may suggest an important role of the dipole–dipole interaction in the vicinity of the phase transition. This kind of interaction becomes more pronounced for the chlorine salts in comparison to that in the bromine ones.

One should also note that the dielectric response of the PCA and PCB crystals resembles to a large extent the dielectric characteristic ($\epsilon(T)$) encountered, for instance, in the improper ferroelectric salts $M_3B_7O_{13}X$ (where M = Mg, Ni, Co, Fe . . ., X = Cl, Br, I) [17] and in the weak (proper) ferroelectrics [18]. The steplike anomaly appears between two ferroelectric phases, for example, in 4-NH_2PyHSbCl_4, as well [11].

The most spectacular feature of the title crystals, PCA and PCB, is the pyroelectric response in the close vicinity of the paraelastic–ferroelastic transition. The spontaneous polarization changes, $|\Delta P_s|$, accompanying these phase transitions, of the order of 1×10^{-4} C m^{-2}, are characteristic of 'weak' ferroelectric crystals.

Acknowledgments

This work was supported by the Polish State Committee for Research (project register number 3T09A 023 26). The authors also thank Professor Piotr Zieliński for stimulating discussions.

References

[1] Jakubas R and Sobczyk L 1990 *Phase Transit.* **20** 163
[2] Sobczyk L, Jakubas R and Zaleski J 1997 *Pol. J. Chem.* **71** 265
[3] Mróz B, Tuszyński J A, Kiefte H, Clouter M J, Jakubas R and Sept D 1997 *Phys. Rev.* B **58** 14261
[4] Kawai T, Takao E, Shimanuki S, Iwata M, Miyashita A and Ishibashi Y 1999 *J. Phys. Soc. Japan* **68** 2848
[5] Hashimoto M, Hashimoto S, Terao H, Kuma M, Niki H and Ino H 2002 *Z. Naturf.* a **55** 167
[6] Wojtaś M, Bator G, Jakubas R, Zaleski J, Kosturek B and Baran J 2003 *J. Solid State Chem.* **173** 425
[7] Jakubas R, Czapla Z, Galewski Z, Sobczyk L, Zogał O J and Lis T 1986 *Phys. Status Solidi* a **93** 449
[8] Kallel A and Bats J 1985 *Acta Crystallogr.* C **51** 1022
[9] Lazarini F 1977 *Acta Crystallogr.* B **33** 2686
[10] Jóźków J, Jakubas R, Bator G and Pietraszko A 2001 *J. Chem. Phys.* **114** 7239
[11] Jakubas R, Bator G and Ciunik Z 2003 *Phys. Rev.* B **64** 024103
[12] Sheldrick G M 1997 *SHELXS97: Program for the Solution of Crystal Structure* University of Göttingen, Germany
[13] Sheldrick G M 1997 *SHELXL97: Program for the Refinement of Crystal Structure* University of Göttingen, Germany
[14] Hubbard C H and Jacobson R 1972 *Inorg. Chem.* **11** 2247
[15] Sapriel J 1975 *Phys. Rev.* B **12** 5128
[16] Wojtaś M, Jakubas R, Ciunik Z and Medycki W 2004 *J. Solid State Chem.* **177** 1575
[17] Smutny F and Fousek J 1970 *Phys. Status Solidi* **40** K13
[18] Blum D, Peuzin J C and Henry J Y 1984 *Ferroelectrics* **69** 283